Giant slip length at a supercooled liquid-solid interface

Suzanne Lafon,[1,*] Alexis Chennevière,[2] Frédéric Restagno,[1] Samy Merabia,[3] and Laurent Joly[3]
[1]*Paris-Saclay University, CNRS, Solid State Physics Laboratory, 91405 Orsay, France*
[2]*CEA Saclay, Léon Brillouin Laboratory, 91191 Gif-sur-Yvette, France*
[3]*Univ Lyon, Univ Claude Bernard Lyon 1, CNRS, Institut Lumière Matière, F-69622 Villeurbanne, France*

(Received 26 July 2022; accepted 10 January 2023; published 6 February 2023)

The effect of temperature on friction and slip at the liquid-solid interface has attracted attention over the last 20 years, both numerically and experimentally. However, the role of temperature on slip close to the glass transition has been less explored. Here we use molecular dynamics to simulate a bidisperse atomic fluid, which can remain liquid below its melting point (supercooled state), to study the effect of temperature on friction and slip length between the liquid and a smooth apolar wall in a broad range of temperatures. At high temperatures, an Arrhenius law fits well the temperature dependence of viscosity, friction, and slip length. In contrast, when the fluid is supercooled, the viscosity becomes super-Arrhenian, while interfacial friction can remain Arrhenian or even drastically decrease when lowering the temperature, resulting in a massive increase of the slip length. We rationalize the observed superlubricity by the surface crystallization of the fluid, and the incommensurability between the structures of the fluid interfacial layer and of the wall. This study calls for experimental investigation of the slip length of supercooled liquids on low surface energy solids.

DOI: 10.1103/PhysRevE.107.025101

I. INTRODUCTION

In 1823 Navier [1] postulated the existence of a velocity jump at the liquid-solid interface and proposed a linear relation between the interfacial stress and the velocity jump: $\tau_{LS} = \lambda V_s$, where λ is the interfacial friction coefficient and V_s is the velocity jump, also called the slip velocity. Because of stress continuity, this is equal to the bulk shear stress $\tau_{bulk} = \eta\dot{\gamma}$, with η the fluid viscosity and $\dot{\gamma}$ the shear rate for sufficiently low shear rates [2]. A more classical way of characterizing slip at the solid-liquid interface is to introduce the slip length b, which is the length at which the velocity profile of the liquid linearly extrapolates to the velocity of the wall [3], leading to

$$b = \frac{V_s}{\dot{\gamma}} = \frac{\eta}{\lambda}. \tag{1}$$

The slip length b is thus dependent on the liquid-surface interaction through the friction coefficient λ. Since both the viscosity η and the friction coefficient λ depend on temperature, so does the slip length b. However, η and λ are both decreasing functions of temperature, thus the resulting effect of temperature on the slip length is not trivial.

In the literature various behaviors of $b(T)$ have been observed. Experimentally, Bäumchen *et al.* [4] reported a decreasing $b(T)$ for PS thin films, while Drda and Wang [5] observed an almost constant slip length for PE melts. Using molecular dynamics (MD) simulations, Servantie and Müller [6] reported nonmonotonic variations of the slip length of a Lennard-Jones (LJ) polymer, and Herrero *et al.* [7] measured a decreasing $b(T)$ for water and methanol on different types of surfaces. In addition, Andrienko *et al.* [8] predicted a jump of the slip length at low temperatures because of prewetting transition at the interface between a binary mixture and a solid wall.

Different models have been proposed in order to rationalize the temperature dependence of the viscosity η, the friction coefficient λ, and the slip length b. A simple description is Eyring's theory, which assumes that flow is an activated process: in order to jump from one position to a neighboring one, a given molecule has to overcome an energy barrier E_a. Although it has been shown that the real microscopic dynamics is not a barrier-hopping mechanism [9,10], Eyring's theory is still useful to compare the general temperature dependency of η and λ in ordinary liquids. It can be applied both to the bulk flow, leading to an Arrhenian viscosity $\eta \propto \exp[E_{a,viscous}/(k_B T)]$ [11], and to the flow near the wall, leading to an Arrhenian friction coefficient $\lambda \propto \exp[E_{a,friction}/(k_B T)]$ [12,13]. Therefore, the slip length also follows an Arrhenius law [11,14–17], which can be expressed as

$$b \propto \exp\left(\frac{E_{a,viscous} - E_{a,friction}}{k_B T}\right), \tag{2}$$

and one cannot know *a priori* its variation with temperature. Recently, Hénot *et al.* [18] have used this formalism to discuss the effect of temperature on the slip length of PDMS melts measured with a velocimetry technique. Equation (2) fits well their data, and depending on the surface, $E_{a,friction}$ was either larger than or equal to $E_{a,viscous}$, implying that the slip length was increasing or constant with temperature, respectively.

However, this Arrhenius picture is not always accurate, especially for supercooled liquids. Indeed, near the glass

*suzanne.lafon@universite-paris-saclay.fr

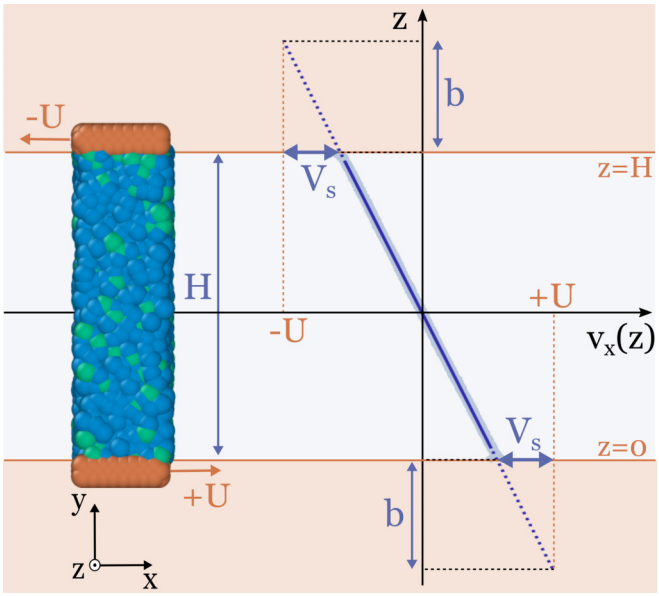

FIG. 1. Schematic of the simulated system and corresponding flow profile $v_x(z)$ of the liquid. The bottom (top) wall has a velocity $+U$ $(-U)$ along the x direction. The distance between the walls is denoted H. The slip length b is defined as the length at which the velocity profile extrapolates to the velocity of the wall. The slip velocity V_s is the velocity difference between the velocity of the liquid at the wall and the velocity of the wall.

transition, the viscosity increases much more sharply than an Arrhenian dependency. To account for this quick increase, other models have been proposed, among them the Vogel-Fulcher-Tammann (VFT) law [19–21], which states that $\eta \propto \exp[A/(T - T_{\rm VFT})]$, with $T_{\rm VFT}$ a reference temperature at which the viscosity diverges. This law is widely used to describe the temperature dependence of the viscosity close to the glass transition, and it has also been used to describe the temperature dependence of the friction coefficient [7].

In this article we present MD computations of the slip length of a model bidisperse LJ liquid in a wide range of temperatures. Far from the glass transition temperature, we show that the slip length is Arrhenian with an effective activation energy controlled by the strength of the liquid-solid (L-S) interaction: $b(T)$ decreases with temperature for weak L-S coupling, while it increases with temperature for strong interaction with the wall. At lower temperatures, the slip length may increase by orders of magnitude as a result of the super-Arrhenian behavior of the viscosity, and the Arrhenian or even sub-Arrhenian behavior of the friction coefficient. In particular, for weakly interacting surfaces, the first liquid layers become structured, and the incommensurability between the fluid local structure and the wall lattice results in a strong reduction of the L-S friction, and thus giant values of the slip length.

II. METHODS

We perform MD simulations using the LAMMPS package [22]. We simulate a shear flow of a Kob-Andersen (KA) binary LJ liquid [23] sheared between two LJ walls (see Fig. 1). We use the KA liquid described in [24], which is a mixture of two particle types $i = $ A, B in a 80-20 ratio. They interact through a LJ pair potential $V_{ij}(r) = 4\varepsilon_{ij}[(\sigma_{ij}/r)^{12} - (\sigma_{ij}/r)^6]$, with $\varepsilon_{\rm AA} = \varepsilon$ and $\sigma_{\rm AA} = \sigma$ taken as references. In the following, all quantities are reported in LJ reduced units, using ε, σ, and the particle mass m as units of energy, distance, and mass, respectively, and taking $k_{\rm B} = 1$. All the atoms are supposed to have the same mass m, and we take $\sigma_{\rm BB} = 0.88$, $\sigma_{\rm AB} = 0.80$, $\varepsilon_{\rm BB} = 0.50$, and $\varepsilon_{\rm AB} = 1.50$. The potential is truncated and shifted to zero at $r_{\rm c} = 2.5$. The wall is a crystallized face-centered cubic (FCC) lattice of type C particles with a lattice parameter $a = 1$, corresponding to a number density $\rho = 4.0$. The effect of the wall density on slip is discussed in Fig. 10 in Appendix A. The strength of the liquid-solid interaction potential $\varepsilon_{\rm AC} = \varepsilon_{\rm BC} \equiv \varepsilon_{\rm LS}$ is varied from 0.15 to 1.00, and we take $\sigma_{\rm AC} = \sigma_{\rm BC} = 1.00$ for all the simulations. The wall dimensions are $L_x = L_y = 8.0$ with periodic boundary conditions in both x and y directions.

The temperature is imposed using a Nosé-Hoover thermostat with a damping time of 100 time steps. When the liquid is sheared, the thermostat is coupled only to transverse velocities. The pressure is set to 10.0 by using the top wall as a piston during a preliminary run. This is a standard choice of pressure for a Kob-Andersen liquid [23,24], and we have checked that the pressure did not impact the slip length significantly (see Fig. 9 in Appendix A). The top wall is then fixed at its equilibrium position. From this equilibrated system, we use two different procedures to measure η and λ. In the first one, the walls are displaced along the x axis at constant velocity $\pm U$. We record the velocity profile of the liquid $v_x(z)$ (Fig. 1) and the stress exerted by the liquid on the walls τ_{LS}. The viscosity η is calculated with $\eta = \tau_{\rm LS}/\dot{\gamma}$, with $\dot{\gamma}$ being the shear rate extracted from the velocity profile. We measure the hydrodynamic height h using the Gibbs dividing plane (GDP) method described in [25]; see Fig. 7 in Appendix A. The friction coefficient λ is then calculated by $\lambda = \tau_{\rm LS}/V_{\rm s}$, with the slip velocity $V_{\rm s} = U - \dot{\gamma}h/2$. The shear velocity U is varied between 0.001 and 1.20, and the values of η and λ are taken in the linear response regime (see Fig. 8 in Appendix A).

For a given system, we plot the velocity profile [see Fig. 2(a)]. At low temperatures, the velocity profile evolves with time. We attribute this time dependency to the consequence of a very high slip length, which allows the liquid to diffuse in block, adding a random constant velocity to the shear flow. However, the slope $\dot{\gamma} = \frac{\partial v}{\partial z}$ is approximately constant over time. We measure the shear rate at different times and for systems having identical parameters but different initial conditions [see Fig. 2(b)]. Then the shear rate at a given $(T, \epsilon_{\rm LS})$ is taken as the mean value of the shear rates at all times for all measurements done in the linear response regime. The error bars correspond to the standard deviation of these measurements divided by the square root of the number of measurements and enlarged by the Student factor.

The second procedure consists in measuring both parameters at equilibrium using Green-Kubo relations [9,26]. For the viscosity one uses

$$\eta = \frac{V}{k_B T}\frac{1}{5}\sum_i \lim_{t\to+\infty}\int_0^t \langle\sigma_i(0)\sigma_i(\tau)\rangle\, d\tau, \qquad (3)$$

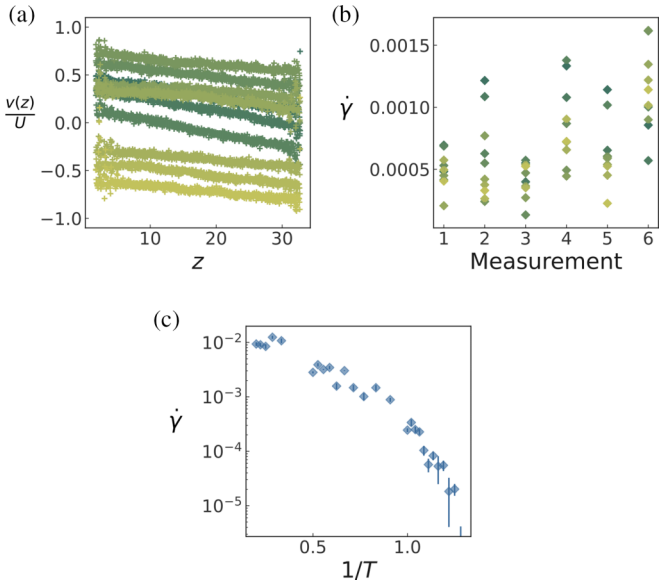

FIG. 2. (a) Velocity profiles for one given measurement at $U = 0.10$, $T = 0.90$, and $\epsilon_{\rm LS} = 0.25$. The colors correspond to different times during shear. (b) Shear rate $\dot{\gamma}$ for different measurements performed in the same conditions. The velocity profiles plotted on the left correspond to measurement 4 in this figure. (c) Shear rate as a function of $1/T$, measured in the Newtonian regime at $\epsilon_{\rm LS} = 0.25$.

where V is the volume, $k_{\rm B}$ is the Boltzmann constant (here taken equal to 1), T is the temperature of the system, and $\sigma_i = \sigma_{xy}, \sigma_{xz}, \sigma_{yz}, (\sigma_{xx} - \sigma_{yy})/2, (\sigma_{yy} - \sigma_{zz})/2$ are the traceless components of the stress tensor inside the liquid and are measured in an independent, fully periodic simulation. For the friction coefficient, one uses

$$\lambda = \frac{S}{k_B T}\frac{1}{2}\sum_j \lim_{t\to+\infty}\int_0^t \langle\sigma_j(0)\sigma_j(\tau)\rangle\, d\tau, \qquad (4)$$

where $S = L_x L_y$ is the surface, and the $\sigma_j = \sigma_{\rm LS,\,top}, \sigma_{\rm LS,\,bottom}$ are the liquid-solid friction forces per unit surface along the x direction at the two liquid-solid interfaces.

III. HIGH-TEMPERATURE REGIME ($T \geqslant 1.5$)

The results are shown in Fig. 3. At high temperatures, both the equilibrium and the nonequilibrium procedures give the same results for the viscosity and the friction coefficient. Both η and λ can be fitted by an Arrhenius law $\eta \propto \exp(E_{\rm a,viscous}/T)$ and $\lambda \propto \exp(E_{\rm a,friction}/T)$, with a friction activation energy $E_{\rm a,friction}$ which depends on the strength of the liquid-solid interaction $\epsilon_{\rm LS}$.

We depict in Fig. 4(a) the slip length of the KA mixture as a function of temperature and for different values of the L-S interaction strength ε_{LS}. In this regime, we restrain ourselves to temperatures larger than the glass transition temperature $T_{\rm g}$, which we estimated to be $T_{\rm g} \simeq 0.41 \pm 0.01$ using a VFT regression of the viscosity temperature dependence [19–21] (see below). We find an activation energy $E_{\rm a}$ of 2.78 for the viscosity and between 1.79 and 4.39 for the friction coefficient, depending on $\varepsilon_{\rm LS}$.

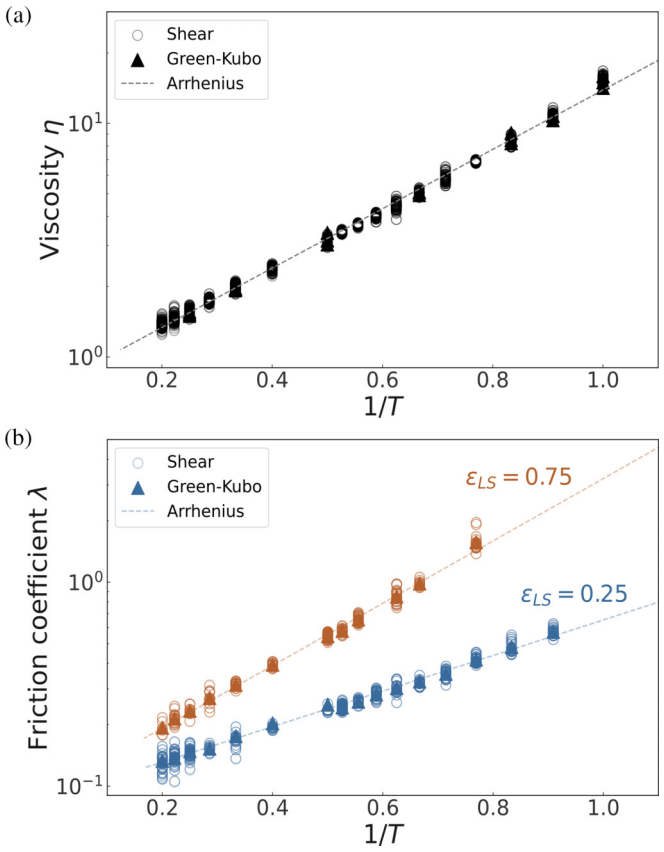

FIG. 3. Viscosity η and friction coefficient λ as a function of temperature measured by shear (empty circles) and at equilibrium using Green-Kubo relations (filled triangles). Both methods give the same values. The friction coefficient measurement is illustrated here for two different values of the liquid-solid interaction energy $\varepsilon_{\rm LS} = 0.25$ (blue) and $\varepsilon_{\rm LS} = 0.75$ (orange). The dotted lines correspond to Arrhenius regressions.

The slip length $b(T)$ being given by the ratio η/λ, it can be fitted by an Arrhenius law $b(T) \propto \exp(E_{\rm a,slip}/T)$, with a formal activation energy of slip $E_{\rm a,slip} = E_{\rm a,viscous} - E_{\rm a,friction}$, which can be either positive or negative. Therefore, $b(T)$ can be increasing or decreasing with temperature depending on the relative values of $E_{\rm a,viscous}$ and $E_{\rm a,friction}$. We plot $E_{\rm a,slip}$ as a function of the L-S interaction energy $\varepsilon_{\rm LS}$ in Fig. 4(b). For high values of $\varepsilon_{\rm LS}$, $E_{\rm a,friction}$ becomes larger than $E_{\rm a,viscous}$. Thus, far from the glass transition temperature, the variation of $b(T)$ is governed by the parameter $\varepsilon_{\rm LS}$, which controls the wettability of the system. This is consistent with previous work on LJ liquids [17].

IV. LOW-TEMPERATURE REGIME ($T \leqslant 1.5$)

We now explore lower temperatures. At these temperatures, the measurement of the friction coefficient λ using the Green-Kubo formula becomes delicate because of the so-called plateau problem [27,28]. Therefore, in this regime, λ is measured with shear simulations only. The viscosity is independent of the value of $\varepsilon_{\rm LS}$, as observed in the inset of Fig. 5(b) where the points correspond to measurements at different $\varepsilon_{\rm LS}$. At high temperatures, $\eta(T)$ is well described by an

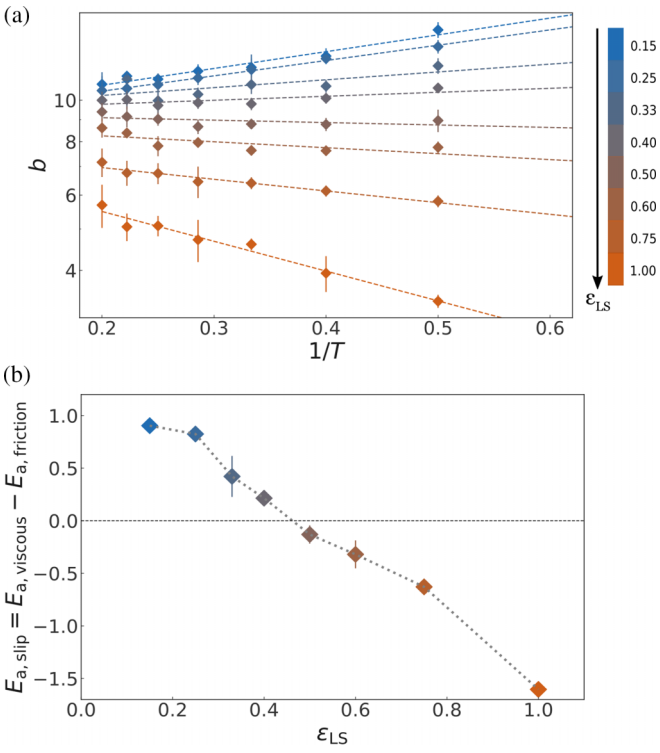

FIG. 4. (a) Temperature dependence of the slip length for different liquid-wall interaction energies ε_{LS}. The dotted lines correspond to Arrhenius-like regressions, from which we extract an activation energy for the slip length $E_{a,slip}$. (b) Activation energy of the slip length as a function of ε_{LS}. The dotted line is a guide for the eye. At small ε_{LS} (nonwetting case), the activation energy of viscosity is higher than the one of friction, so that $E_{a,slip} > 0$ and b decreases with T. In contrast, at high ε_{LS} (wetting case), the activation energy of friction overcomes the one of viscosity, so that $E_{a,slip} < 0$ and b increases with T. A linear regression of this curve gives $E_{a,slip} \approx -2.94(\varepsilon_{LS} - 0.48)$.

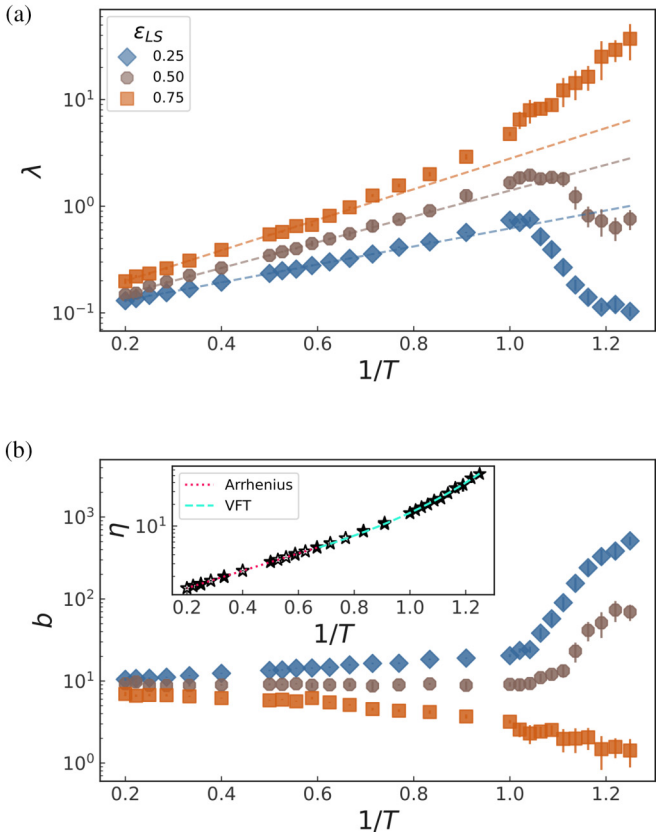

FIG. 5. Temperature dependence of (a) the friction coefficient $\lambda(T)$ and (b) the slip length $b(T)$, derived from $b(T) = \eta(T)/\lambda(T)$. The viscosity $\eta(T)$ is shown in the inset. The dotted lines correspond to Arrhenian regressions at high temperatures. For $\lambda(T)$ and $b(T)$, the colors correspond to different values of ε_{LS} with the same scale as in Fig. 4. For the sake of visibility, only $\varepsilon_{LS} = 0.25$ (blue), 0.50 (brown), and 0.75 (orange) are shown. For small values of ε_{LS}, the friction coefficient drops drastically upon cooling the liquid, so that the slip length b increases sharply.

Arrhenius law (red curve), while at lower temperatures, $\eta(T)$ can be fitted with a VFT model (blue curve) [19–21]: $\eta = \exp(A + \frac{B}{T - T_{VFT}})$ with $A = 0.27 \pm 0.06$, $B = 1.45 \pm 0.06$, and $T_{VFT} = 0.41 \pm 0.01$. For the friction coefficient λ, we focus on a subset of values for ε_{LS} (0.25, 0.50 and 0.75) for clarity. We observe two different behaviors. For $\varepsilon_{LS} = 0.75$, λ becomes super-Arrhenian while decreasing the temperature below 1.5. This slightly overcomes the increase of η upon cooling and thus results in a slip length which keeps decreasing while approaching the glass transition. However, for $\varepsilon_{LS} = 0.25$ and 0.50, the friction coefficient suddenly drops by at least one order of magnitude for $T < 1$. This corresponds to a strong increase of the slip length at low temperatures by more than one order of magnitude.

Servantie and Müller [6] observed the same behavior for the slip length of a LJ polymer slipping on a LJ surface and attributed it to a difference of mobility between the bulk and the interfacial liquid. In addition, Herrero *et al.* [7] studied the slip length of water on graphene and LJ walls. They observed a moderate increase of the slip length at low temperatures for water on LJ walls and a strong increase of b for water on graphene, and related them to subtle differences in the temperature evolution of the static and dynamic contributions to viscosity and friction.

To further explore this point, and to understand the fast decrease of λ at low temperatures, we have calculated the two-dimensional structure factor $S_{liq}(\vec{q})$ of the interfacial liquid and compared it to the structure factor $S_{wall}(\vec{q})$ of the solid wall. The structure factor is calculated by

$$S(\vec{q}) = \frac{1}{N}\left[\left(\sum_{i=0}^{N}\cos(\vec{r}_i \cdot \vec{q})\right)^2 + \left(\sum_{i=0}^{N}\sin(\vec{r}_i \cdot \vec{q})\right)^2\right], \quad (5)$$

where $\vec{r}_i = x_i\vec{e}_x + y_i\vec{e}_y$ is the position of atom i and N is the total number of atoms considered in the calculation (in the first layer of liquid near the wall, delimited by the first nonzero minimum in the density profile in the z direction). The values of q at which we calculate the structure factor are multiples of $2\pi/L$ with L the size of the box in x and y directions. The commensurability between the local structure of the liquid interfacial layer and the wall structure is a key factor controlling friction. This commensurability can be quantified by the value of the two-dimensional structure factor of the liquid

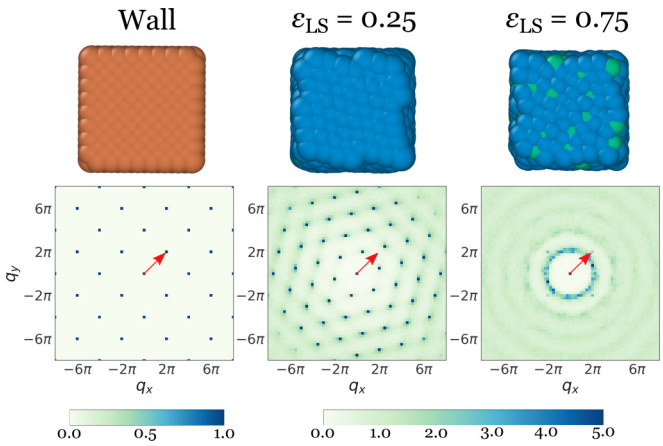

FIG. 6. Structure factors of the wall (left) and of the interfacial liquid (middle: $\varepsilon_{LS} = 0.25$ and right: $\varepsilon_{LS} = 0.75$) at $T = 0.8$, and the corresponding snapshots of the structure (top). The red arrows indicate $\vec{q}_{wall}$, i.e., the vector $\vec{q}$ corresponding to the first peak in the wall structure factor. For small L-S interaction strengths ($\varepsilon_{LS} = 0.25$), B particles are expelled from the interface, and the remaining A particles close to the wall structure themselves into a hexagonal lattice, while the wall displays a square structure. Because these two lattices are incommensurate, the friction is highly reduced, leading to very large slip lengths. However, at high L-S interaction strengths ($\varepsilon_{LS} = 0.75$), B particles remain at the interface and prevent the near-wall liquid to structure itself; hence the friction remains large and the slip length increases only moderately.

interfacial layer at the smallest characteristic wave vector of the wall interaction energy landscape, $S_{liq}(\vec{q}_{wall})$, where $\vec{q}_{wall}$ is the position of the first peak in the wall structure factor [29,30].

The results are shown in Fig. 6. For $\varepsilon_{LS} = 0.25$, in the snapshot of the interface, one can see that type B particles are depleted from the interface, allowing the liquid near the wall to structure itself into a lattice, which turns out to be hexagonal. We have quantified this depletion of B particles near the wall in Fig. 12 in Appendix B, where we plot the concentration of A particles near the wall against temperature. For low values of ε_{LS} at low temperatures, the concentration of A particles at the interface is close to 100%, which allows the corresponding liquid layers to crystallize. Because the wall displays an incommensurate square lattice, the liquid structure factor is very small at the position $\vec{q}_{wall}$ of the first peak of the wall structure factor, i.e., $S(\vec{q}_{wall}) \ll 1$, and the friction coefficient λ is strongly reduced. It is worth noting that the lattice of the interfacial liquid displays an hexagonal order both at equilibrium and under shear, at any considered velocity (see Fig. 11 in Appendix B). In contrast, for stronger L-S interaction ($\varepsilon_{LS} = 0.75$), type B particles remain at the interface and prevent the interfacial liquid to structure itself, and thus its structure factor remains that of a liquid. In this case, $S(\vec{q}_{wall})$ remains on the order of 1, and the friction coefficient still increases in an Arrhenian way upon cooling down the liquid, which results in a moderate increase of the slip length.

Here superlubricity is possible because of the structure of the interface and is reminiscent of solid-solid superlubricity, as evidenced experimentally, e.g., for graphite [31]. Indeed, the role of incommensurability in reducing the friction between two solids has been reported by Zhang *et al.* [32] and Franchini *et al.* [33] for Al/Al and Xe/Cu interfaces, respectively. In addition, Cieplak *et al.* [34] have observed a strong reduction of friction from a fluid to a crystallized layer of krypton adsorbed on gold because of incommensurability between the crystallized krypton layer and the gold lattice.

V. CONCLUSION

In conclusion, the MD investigation of $b(T)$ has revealed that at high temperatures not only the viscosity but also the friction coefficient follow an Arrhenius law. Therefore, the slip length may be also described by an Arrhenius law with an effective activation energy that can be either positive or negative depending on the strength of the liquid-solid interaction potential ε_{LS}. This result aligns well with the prediction for polymer melts described in [18].

A more striking phenomenon is that, at lower temperatures, the slip length may increase by orders of magnitude. This massive enhancement is the result of both the super-Arrhenian temperature dependence of the viscosity in the supercooled regime and the sub-Arrhenian behavior of friction with cooling. In particular, for weak L-S interactions, the friction coefficient is highly reduced due to the emergence of a local fluid structure, which is incommensurate with the solid lattice. These conditions are highly favorable to observe giant values of the slip length. For stronger L-S interactions, the friction coefficient increases in a super-Arrhenian way, resulting in merely a moderate decrease of the slip length. These results showing a possible mechanism for massive slippage on low-energy surfaces could lead to promising transport applications in nanofluidics, and call for experiments probing the slip length at supercooled liquid-solid interface. Short polymer melts close to their glass transition temperature flowing over weakly interacting surfaces are good candidates to evidence massive temperature-dependent slip lengths.

ACKNOWLEDGMENTS

The authors thank Cecilia Herrero, Etienne Fayen, and Patrick Judenstein for fruitful discussions. We are also grateful for HPC resources from GENCI/TGCC (Grant No. A0090810637), from the PSMN mesocenter in Lyon, and from the THEO group in the LPS, Orsay. We thank the ANR POILLU (Grant No. ANR-19-CE06-007) as well.

APPENDIX A: MEASUREMENT OF VISCOSITY AND FRICTION COEFFICIENT

1. Measurement under shear

When a liquid is sheared by two walls, its viscosity is determined through $\eta = \tau_{LS}/\dot{\gamma}$, with τ_{LS} being the stress exerted by the liquid on the walls and $\dot{\gamma}$ being the shear rate extracted from the velocity profile. Then the friction coefficient is measured by $\lambda = \tau_{LS}/V_s$, with the slip velocity $V_s = U - \dot{\gamma}h/2$ where h is the hydrodynamic height of the system. Herrero *et al.* [25] have shown that h can be computed by identifying the hydrodynamic wall position with the Gibbs dividing plane

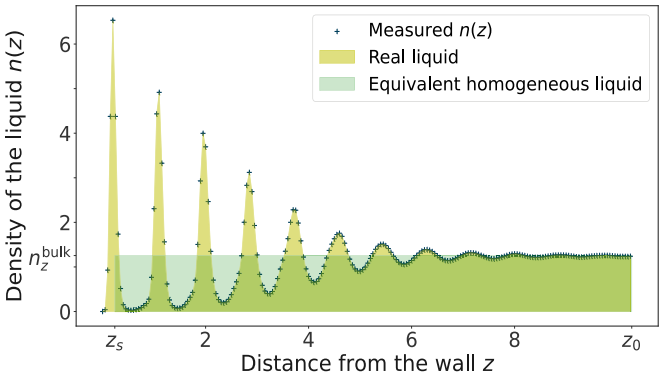

FIG. 7. Density profile of the liquid near the bottom wall. Close to the wall, the density profile displays oscillations. The dots represent measured values of the density, while the light green area represents the integral of the density between 0 and some reference height in the bulk z_0. The dark green area represents a homogeneous liquid containing the same number of atoms as the real liquid. The GDP z_s is determined by equating the light green and the dark green areas.

(GDP). The way we determine the GDP is illustrated in Fig. 7. Near the walls, the density profile $n(z)$ oscillates. The number of particles between the wall and a given height z_0 inside the bulk is calculated by integrating the liquid density $n(z)$ between 0 and z_0: $N = \int_0^{z_0} n(z)\,dz$. A homogeneous distribution of these N atoms would lead to $N = n_z^{\text{bulk}}(z_0 - z_s)$ with z_s the GDP position. By equating these two equations, one can calculate z_s:

$$z_s = z_0 - \frac{\int_0^{z_0} n(z)\,dz}{n_z^{\text{bulk}}}. \tag{A1}$$

At sufficiently low shear rate $\dot{\gamma}$, the slip length is constant, while at high shear rates, the Navier condition fails and the slip length increases rapidly with $\dot{\gamma}$. We want to stay in the linear response regime, so, for each system, we apply various shear velocities U to determine the threshold velocity above which we leave the Navier regime. In practice, we measure the viscosity η and the friction coefficient λ. At low U, we have a plateau while at high U, both η and λ decrease. We computed the value of the threshold shear velocity for

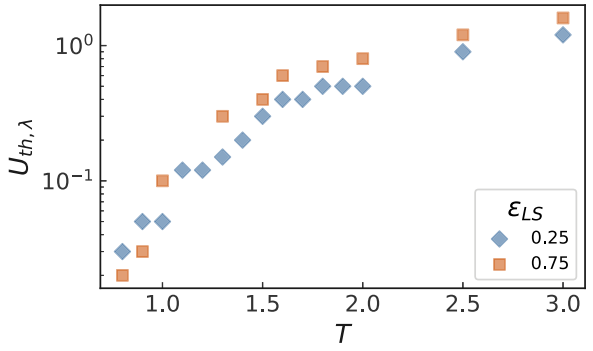

FIG. 8. Threshold shear velocity $U_{\text{th},\lambda}$ as a function of temperature for two different values of the liquid-solid interaction strength ϵ_{LS}. Both the liquid viscosity η and the friction coefficient λ are independent of the shear velocity U for $U \leqslant U_{\text{th},\lambda}$.

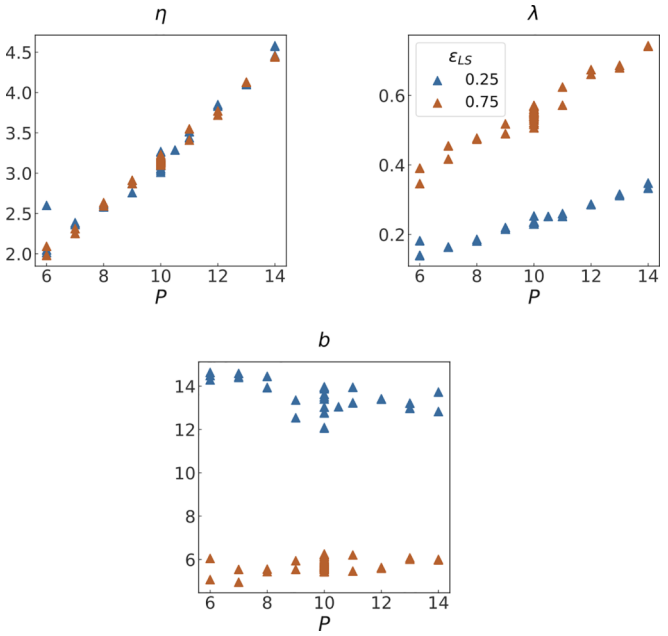

FIG. 9. Effect of pressure on the slip length. The measurements have been done for a sheared liquid at $U = 0.40$ and $T = 2.0$.

both η and λ. The threshold velocity was smaller for λ than for η, therefore we kept only this one as an upper bound for the shear velocity. In Fig. 8 we plot the threshold velocity for λ and the corresponding threshold shear rate as a function of temperature and L-S interaction strength.

We do at least three different measurements for each data point shown in the results. At low temperatures ($T \leqslant 1$), the threshold velocity becomes very small, so the curves become noisy, and therefore we do at least six different measurements for each data point.

2. Effect of pressure on slip length

For all the simulations, we have chosen a pressure $P = 10.0$. This is a standard choice for a Kob-Andersen liquid. We have tested the effect of pressure on the slip length for

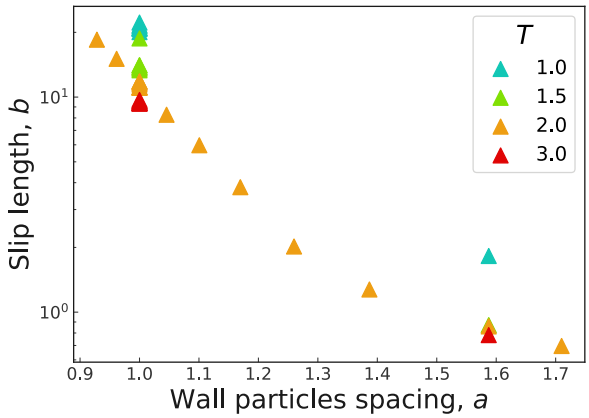

FIG. 10. Effect of wall particles spacing on the slip length. The measurements have been done for $\varepsilon_{\text{LS}} = 0.25$ using Green-Kubo simulations.

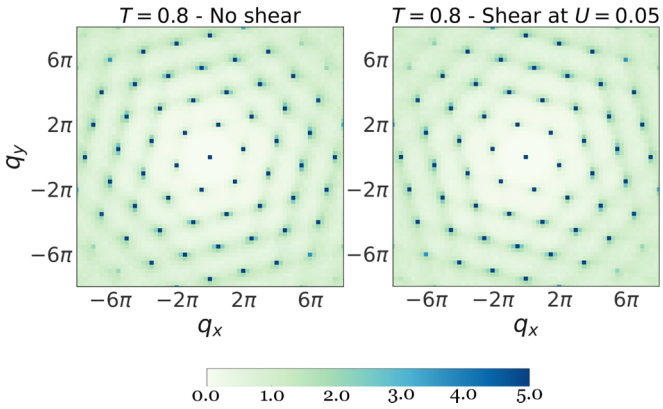

FIG. 11. Comparison of the structure factor of the interfacial liquid. Left: $T = 0.8$ without shearing the liquid. Right: with shearing the liquid at $U = 0.05$. The structure of the liquid layer in contact with the wall remains hexagonal both at rest and under shear. The only difference is that the lattice can be rotated.

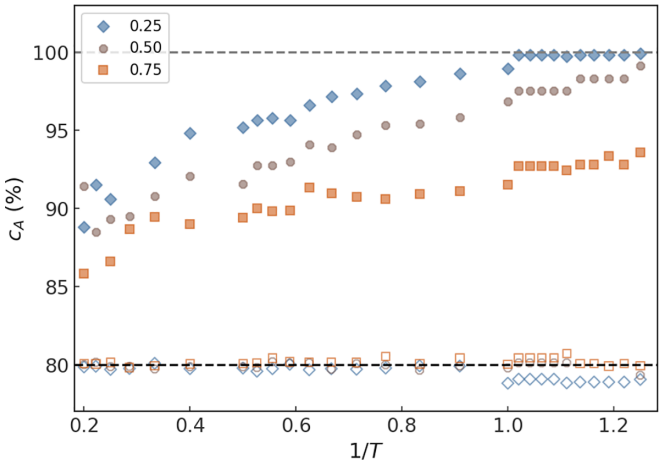

FIG. 12. Concentration of A particles close to the interface, as a function of temperature and for different values of ϵ_{LS}. Empty symbols correspond to concentration of A particles in the bulk.

pressures around our reference $P = 10.0$. The results are shown in Fig. 9. Both the viscosity and the friction coefficient increase rather linearly with the pressure. The slip length, which is the ratio of the two, appears to remain relatively constant in the range of explored pressures.

3. Effect of wall density on slip length

We have studied the evolution of the slip length as a function of the wall particles spacing a, which is related to the reduced wall density $\tilde{\rho}$ through $\tilde{\rho} = 4\sigma^3/a^3$. The result is shown in Fig. 10. We can see that the slip length for $a = 1.0$ (which corresponds to $\tilde{\rho} = 4.0$) is ten times higher than the one for $a \approx 1.6$ (which corresponds to $\tilde{\rho} = 1.0$).

APPENDIX B: STRUCTURATION AT THE LIQUID-SOLID INTERFACE AT LOW T

1. Structure factors

We calculate the structure factor of the first liquid layer in contact with the solid wall, for systems under shear or at rest, and for various temperatures. We observe that a hexagonal lattice appears at low temperatures for weak liquid-solid interaction strengths. The structure of the liquid layer remains hexagonal even under shear (see Fig. 11).

2. Discussion about demixing

In order to explain the crystallization near the wall at low temperatures, we have computed the concentration of A particles c_A near the wall as a function of temperature. For each measurement, we compute the position of the first liquid atoms z_{min} near the wall and we define a layer of thickness 0.1 inside which we calculate the concentrations. c_A is defined as $c_A = N_A^{interface}/N^{interface}$ where $N_A^{interface}$ ($N^{interface}$) is the number of A particles (the total number of particles) in this first liquid layer. The result is shown in Fig. 12. We observe that c_A near the interface is always larger than in the bulk. In addition, as the temperature decreases, c_A increases and even reaches 100 % at $T \leqslant 1$ for $\varepsilon_{LS} = 0.25$. The ability of the liquid to be supercooled is due to its bidispersity. Therefore, when the liquid becomes almost pure, it cannot maintain its supercooled state and crystallizes.

[1] C. L. Navier, *Mémoire sur les lois du mouvement des fluides* (Académie des Sciences, Paris, 1823).

[2] N. V. Priezjev and S. M. Troian, Molecular Origin and Dynamic Behavior of Slip in Sheared Polymer Films, Phys. Rev. Lett. **92**, 018302 (2004).

[3] C. Neto, D. R. Evans, E. Bonaccurso, H.-J. Butt, and V. S. J. Craig, Boundary slip in Newtonian liquids: A review of experimental studies, Rep. Prog. Phys. **68**, 2859 (2005).

[4] O. Bäumchen, M. Lessel, R. Fetzer, R. Seemann, and K. Jacobs, Sliding fluids: Dewetting experiments reveal the solid/liquid boundary condition, J. Phys.: Conf. Ser. **216**, 012002 (2010).

[5] P. P. Drda and S.-Q. Wang, Stick-Slip Transition at Polymer Melt/Solid Interfaces, Phys. Rev. Lett. **75**, 2698 (1995).

[6] J. Servantie and M. Müller, Temperature Dependence of the Slip Length in Polymer Melts at Attractive Surfaces, Phys. Rev. Lett. **101**, 026101 (2008).

[7] C. Herrero, G. Tocci, S. Merabia, and L. Joly, Fast increase of nanofluidic slip in supercooled water: The key role of dynamics, Nanoscale **12**, 20396 (2020).

[8] D. Andrienko, B. Dünweg, and O. I. Vinogradova, Boundary slip as a result of a prewetting transition, J. Chem. Phys. **119**, 13106 (2003).

[9] J.-P. Hansen and I. R. McDonald, *Theory of Simple Liquids: With Applications to Soft Matter* (Academic Press, Amsterdam, 2013).

[10] F. Rizk, S. Gelin, A.-L. Biance, and L. Joly, Microscopic Origins of the Viscosity of a Lennard-Jones Liquid, Phys. Rev. Lett. **129**, 074503 (2022).

[11] P. F. Pelz and T. Corneli, The activation energy for wall slip, arXiv:2111.09693.

[12] T. D. Blake, Slip between a liquid and a solid: D. M. Tolstoi's (1952) theory reconsidered, Colloids Surf. **47**, 135 (1990).

[13] K. Jacobs, R. Seemann, G. Schatz, and S. Herminghaus, Growth of holes in liquid films with partial slippage, Langmuir **14**, 4961 (1998).

[14] S. Lichter, A. Martini, R. Q. Snurr, and Q. Wang, Liquid Slip in Nanoscale Channels as a Rate Process, Phys. Rev. Lett. **98**, 226001 (2007).

[15] F.-C. Wang and Z. Ya-Pu, Slip boundary conditions based on molecular kinetic theory: The critical shear stress and the energy dissipation at the liquid–solid interface, Soft Matter **7**, 8628 (2011).

[16] G. J. Wang and G. Hadjiconstantinou, Universal molecular-kinetic scaling relation for slip of a simple fluid at a solid boundary, Phys. Rev. Fluids **4**, 064201 (2019).

[17] Z. Guo, T. S. Zhao, and Y. Shi, Temperature dependence of the velocity boundary condition for nanoscale fluid flows, Phys. Rev. E **72**, 036301 (2005).

[18] M. Hénot, M. Grzelka, J. Zhang, S. Mariot, I. Antoniuk, E. Drockenmuller, L. Léger, and F. Restagno, Temperature-Controlled Slip of Polymer Melts on Ideal Substrates, Phys. Rev. Lett. **121**, 177802 (2018).

[19] H. Vogel, Das Temperaturabhaengigkeitsgesetz der Viskositaet von Fluessigkeiten, Phys. Z. **22**, 645 (1921).

[20] G. S. Fulcher, Analysis of recent measurements of the viscosity of glasses, J. Am. Ceram. Soc. **8**, 339 (1925).

[21] G. Tammann and W. Hesse, The dependence of viscosity upon the temperature of supercooled liquids, Z. Anorg. Allg. Chem. **156**, 245 (1926).

[22] A. P. Thompson, H. M. Aktulga, R. Berger, D. S. Bolintineanu, W. M. Brown, P. S. Crozier, P. J. in 't Veld, A. Kohlmeyer, S. G. Moore, T. D. Nguyen *et al.*, LAMMPS—A flexible simulation tool for particle-based materials modeling at the atomic, meso, and continuum scales, Comput. Phys. Commun. **271**, 108171 (2022).

[23] W. Kob and H. C. Andersen, Testing mode-coupling theory for a supercooled binary Lennard-Jones mixture, Phys. Rev. E **51**, 4626 (1995).

[24] U. R. Pedersen, T. B. Schrøder, and J. C. Dyre, Phase Diagram of Kob-Andersen-Type Binary Lennard-Jones Mixtures, Phys. Rev. Lett. **120**, 165501 (2018).

[25] C. Herrero, T. Omori, Y. Yamaguchi, and L. Joly, Shear force measurement of the hydrodynamic wall position in molecular dynamics, J. Chem. Phys. **151**, 041103 (2019).

[26] L. Bocquet and J.-L. Barrat, On the Green-Kubo relationship for the liquid-solid friction coefficient, J. Chem. Phys. **139**, 044704 (2013).

[27] P. Español and I. Zúñiga, Force autocorrelation function in Brownian motion theory, J. Chem. Phys. **98**, 574 (1993).

[28] L. Bocquet, J.-P. Hansen, and J. Piasecki, Friction tensor for a pair of Brownian particles: Spurious finite-size effects and molecular dynamics estimates, J. Stat. Phys. **89**, 321 (1997).

[29] J.-L. Barrat and L. Bocquet, Influence of wetting properties on the hydrodynamic boundary condition at a fluid-solid interface, Faraday Disc. **112**, 119 (1999).

[30] K. Falk, F. Sedlmeier, L. Joly, R. R. Netz, and L. Bocquet, Molecular origin of fast water transport in carbon nanotube membranes: Superlubricity versus curvature dependent friction, Nano Lett. **10**, 4067 (2010).

[31] M. Dienwiebel, G. S. Verhoeven, N. Pradeep, J. W. M. Frenken, J. A. Heimberg, and H. W. Zandbergen, Superlubricity of Graphite, Phys. Rev. Lett. **92**, 126101 (2004).

[32] Q. Zhang, Y. Qi, L. G. Hector, T. Cagin, and W. A. Goddard, Atomic simulations of kinetic friction and its velocity dependence at Al/Al and α- Al_2O^3/α-Al_2O^3 interfaces, Phys. Rev. B **72**, 045406 (2005).

[33] A. Franchini, V. Bortolani, G. Santoro, and K. Xheka, Effects of the commensurability and disorder on friction for the system Xe/Cu, J. Phys.: Condens. Matter **23**, 484004 (2011).

[34] M. Cieplak, E. D. Smith, and M. O. Robbins, Molecular origins of friction: The force on adsorbed layers, Science **265**, 1209 (1994).